AGU ADVANCING EARTH AND SPACE SCIENCE

Geophysical Research Letters

RESEARCH LETTER
10.1029/2022GL098042

Key Points:

- Charge exchange of energetic water group pickup ions with coma water molecules is observed within the solar wind cavity of Comet 67P Churyumov-Gerasimenko
- Rotation of the comet produced variations in the neutral density at the spacecraft causing strong charge-exchange deceleration of the incoming ions within the density peaks
- Recovery to the initial water-group ion beam as minimum neutral densities, again appeared, was shown to result from pickup of thermal ions in the coma

Supporting Information:

Supporting Information may be found in the online version of this article.

Correspondence to:

R. Goldstein,
rgoldstein@swri.edu

Citation:

Goldstein, R., Burch, J. L., Llera, K., Altwegg, K., Rubin, M., Eriksson, A. I., & Nilsson, H. (2022). Observations of modulation of ion flux in the coma of comet 67p/Churyumov-Gerasimenko. *Geophysical Research Letters*, *49*, e2022GL098042. https://doi.org/10.1029/2022GL098042

Received 28 JAN 2022
Accepted 10 MAY 2022

Author Contributions:

Conceptualization: R. Goldstein
Investigation: J. L. Burch
Methodology: R. Goldstein
Resources: R. Goldstein
Validation: J. L. Burch, K. Llera, A. I. Eriksson, H. Nilsson
Writing – original draft: R. Goldstein
Writing – review & editing: R. Goldstein, J. L. Burch

Observations of Modulation of Ion Flux in the Coma of Comet 67P/Churyumov-Gerasimenko

R. Goldstein[1], J. L. Burch[1], K. Llera[1], K. Altwegg[2], M. Rubin[2], A. I. Eriksson[3], and H. Nilsson[4]

[1]Southwest Research Institute, San Antonio, TX, USA, [2]Physikalisches Institut, University of Bern, Bern, Switzerland, [3]Swedish Institute of Space Physics, Uppsala, Sweden, [4]Swedish Institute of Space Physics, Kiruna, Sweden

Abstract On 6–8 June 2015, the Ion and Electron Sensor on board Rosetta observed keV-range water-group pickup ions arriving from the solar direction. Based on magnetic field intensification and variations, the appearance of the ions was likely to have been caused by a coronal mass ejection. During the 3-day period when Rosetta was 200 km from the comet, peak ion energy/charge (E/q) varied over a range from 50 eV to 1 keV in concert with neutral gas density variations caused by the rotation of the comet and its variable solar illumination. Thermal ion densities showed the same variations. The neutral density variations provided a unique opportunity to observe the repeated slowing of the solar wind by mass loading caused by charge exchange between energetic water-group ions and thermal water-group molecules. Such solar wind slowing was observed previously only by flyby missions that provided single events.

Plain Language Summary The Rosetta orbiter carried a number of instruments to measure the properties of the neutral and ionized gas surrounding the nucleus. Included in these were plasma instruments to measure the characteristics of the charged particles. The Ion and Electron Sensor was one of them. Also on board were the Rosetta Orbiter Spectrometer for Ion and Neutral Analysis, the Ion Composition Analyzer, and the Langmuir Probe. This paper discusses some of the results of measurements by these instruments and their relation to each other. It was found that the neutral gas emitted by the comet nucleus and the resulting positively charged ions interact in such a way to produce slowing down of the solar wind as a result of what is called "charge exchange", in which an electron is transferred from a neutral molecule to an ion.

1. Introduction

The Rosetta spacecraft (SC) arrived at comet 67P Churyumov-Gerasimenko (CG) in August 2014 and remained in its vicinity until 30 September 2016, when it landed on the comet and terminated its mission. Perihelion occurred on 13 August 2015 at 1.24 AU from the Sun. Early measurement of plasma at CG, when it was as far as 3.2 astronomical units (AU) from the Sun, showed solar wind ions and electrons along with primarily low-energy cometary H_2O^+, such as reported by Broiles et al. (2015), Goldstein et al. (2015), and Nilsson et al. (2015). These thermal ions result from a combination of solar UV photoionization and electron impact ionization (Galand et al., 2016). At this early period in the mission, the energy of the ions produced was near that of the neutrals emitted by the nucleus, that is, the order of 1 eV (Gulkis et al., 2015). This energy was too low to be detected by either the Ion Composition Analyzer (ICA) (Nilsson et al., 2015) or the Ion and Electron Sensor (IES) (Burch et al., 2007), but because the SC potential was normally negative near CG (as low as −20 V), these low-energy positive ions were attracted to the SC and appeared at the lowest end of the energy scale of these instruments. As the comet increased its activity, the coma became more complex, including the ion-neutral interaction known as charge exchange. Studies of charge exchange between solar wind and CG coma species include Mandt et al. (2019) and Wedlund et al. (2019). Wedlund et al. (2019) noted that charge-exchange reactions play an important role in the inner coma of comet 67P and identified periods when solar wind charge exchange may, for a short time, rival electron ionization frequencies in the production of ions.

As the SC moved closer to the Sun, the solar wind was deflected away from the comet until between 28 April and 15 December 2015; the solar wind protons and He^{++} disappeared completely (Behar et al., 2017) while water-group pickup ions created by mass-loading of the solar wind were still seen. The water-group ions, having higher momentum, were not deflected as much as the protons and He^{++} and so continued to move toward the comet. Nevertheless, as shown by Edberg et al. (2016), during the time period when CG was within the solar wind cavity only low-energy water-group ions were observed except on occasions when coronal mass ejections (CMEs) compressed the solar wind cavity. During these compressions, the water-group beams were observed at keV energies. The time period covered by this report likely occurred during one of these CME impacts, as determined by the turbulent magnetic field signatures, the appearance of antisolar beams of pickedup water group ions (resulting from compression of the coma), and by the appearance of multiple CMEs emitted toward Rosetta over the previous few days as measured by SOHO-LASCO (Brueckner et al., 1995).

The observations during 6–8 June 2015 contained variations of neutral density caused by the rotation of CG (12.4-hr period) and the resulting variation of solar illumination of different parts of the comet. A 6.2-hr periodicity of the neutral density and thermal plasma was reported by Edberg et al. (2015) and Gulkis et al. (2015), who noted that the highest densities are observed above the neck area, that is, the area in between the two main lobes of the comet, which is exposed to solar illumination twice per rotation.

Because of the neutral gas density variations, we were able to explore the evolution from an antisolar beam consisting completely of water-group pickup ions to a low-energy (10s–100 eV) directionally spread ion population resulting from charge exchange of water-group ions with water-group molecules in the collision-dominated coma. In addition to momentum-transfer collisions, the directional spreading is caused by the ion pickup process that starts with acceleration along the motional electric field, which is normal to the flow direction. With this unique situation, we were able to determine the mean free path of the incident ions, which remained larger than their gyroradii throughout the events.

2. Observations

2.1. In Situ Data on 6–8 June 2015

We discuss data for the period 6–8 June 2015, shown in Figure 1, at about 200 km from CG and 1.48 AU from the Sun. As viewed from the Rosetta position, the average azimuth and elevation of CG in Comet-Sun-Equatorial (CSEQ) coordinates (defined in the caption of Figure 1) were 97.23° and 65.00°, respectively, so that the SC was in the Southern Hemisphere near the dusk meridian. This time interval is part of the solar wind exclusion period so the ion interactions do not include solar wind protons and He^{++} but do include pickedup water-group ions. These pickup ions can originate beyond the solar wind cavity, in which case they have E/q in the keV range, or within the solar wind cavity, in which case the E/q is typically a few 10s to a few hundred eV (Goldstein et al., 2015). Reading from top to bottom in Figure 1 are the ion energy fluxes measured by IES; the magnetic field components from the Fluxgate Magnetometer, MAG (Glassmeier et al., 2007); the neutral density from the Rosetta Orbiter Spectrometer for Ion and Neutral Analysis, ROSINA (Balsiger et al., 2007); and the electron density from the Langmuir Probe, LAP (Eriksson et al., 2007). Notable features of Figure 1 include periodic troughs in the ion fluxes, with a period near half the CG rotation rate of 12.4 hr, and the coincidence of those troughs with the peaks of the neutral and electron density. Vertical blue/white lines show the time period of the analysis described in Section 3.

Figures 4 and 5 of Galand et al. (2016) for early October 2014 at 20 km from CG are analogous to Figure 1 except that the Figure 1 data were taken at 200 km from CG and in the solar wind cavity so the solar wind does not appear. The solar wind protons were the most evident ions in 2014, in contrast to the water-group ions appearing in Figure 1 in 2015. But in both cases, ionization of the neutrals from the comet increased the electron density, which in turn drove the SC potential more negative.

Figure S1 in Supporting Information S1 shows measurements from ICA taken during 7 June 2015. There was a data gap during this time period and the operating mode was such that detailed energy spectra were not available. Nevertheless, Figure S1 in Supporting Information S1 shows that all ions measured on this day were water-group ions.

2.2. IES Data During Neutral Density Variation

Figure 2 shows (a) magnetic field magnitude, (b) neutral gas density, and (c–v) ion energy fluxes during one period of the neutral density variations on 7 June 2015. All of the ion plots in Figures 2c–2v contain data summed over elevation channels 4–8. Figures 2c and 2e shows ion count rates (proportional to energy flux) during the time period 07–08 UT as measured by anodes 3–11, which are summed on board because these anodes point toward the Sun and solar wind. Figures 2d and 2f shows the azimuthal distribution of the ion energy flux for all

10.1029/2022GL098042

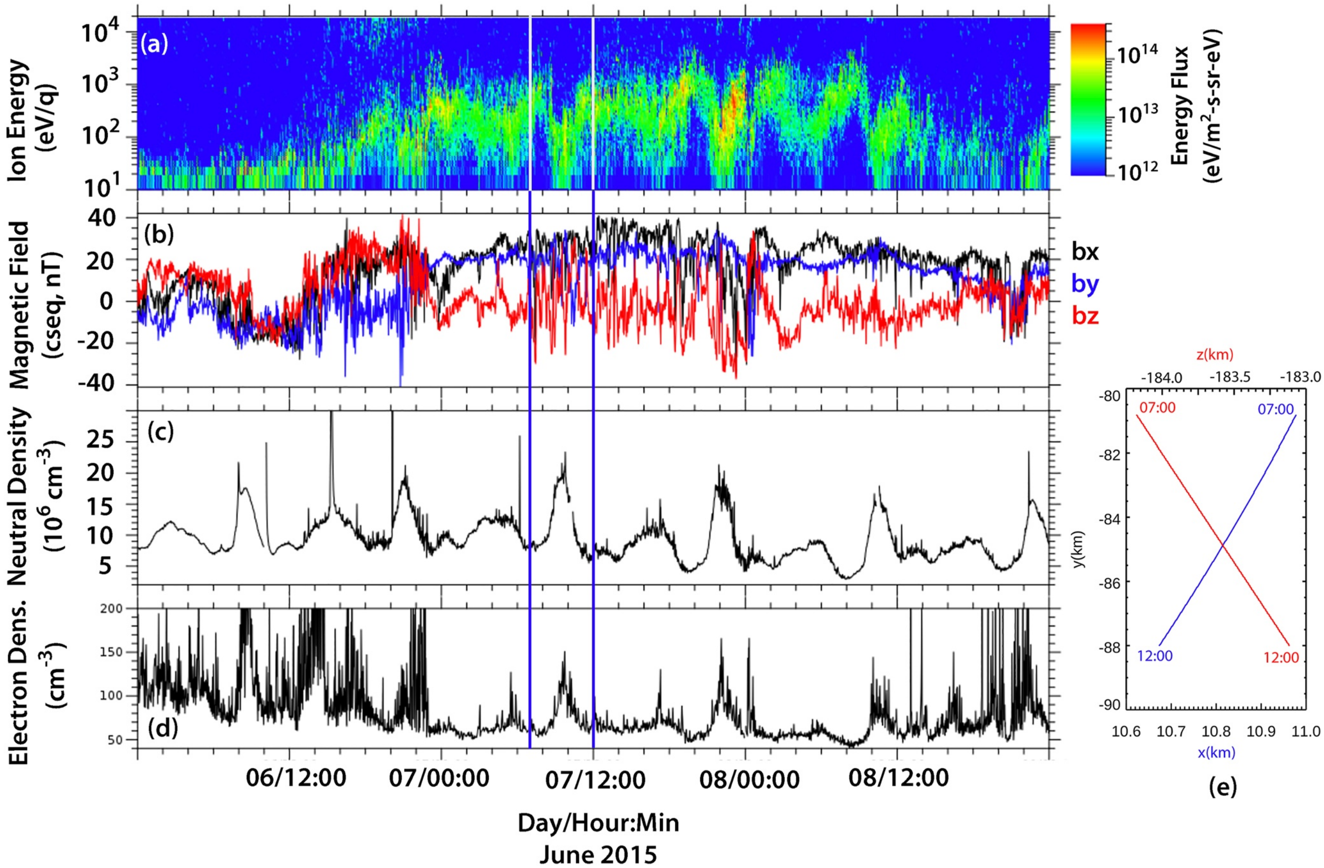

Figure 1. Comparison of measurements of (a) Ion and Electron Sensor ion energy flux, (b) Fluxgate Magnetometer Comet-Sun-Equatorial (CSEQ) magnetic field components in which the *x* axis points toward the Sun, the *z* axis is the component of the Sun's north pole that is orthogonal to the Sun-comet line, and the *y* axis completes the right-handed system; (c) Rosetta Orbiter Spectrometer for Ion and Neutral Analysis neutral density, and (d) Langmuir Probe electron density during the period 6–8 June 2015. The blue/white vertical lines indicate the time period used in the detailed analysis (07–12 UT) with (e) showing the orbit tracks of Rosetta (Data from AMDA).

anodes. Comparison of the corresponding plots in the next four columns shows the evolution of ion distributions as the neutral density rises and then falls. For example, the rightmost column, Figures 2s–2v, is very similar to the leftmost column with ion fluxes peaked in the keV range and concentrated mostly from the solar direction. The middle three columns show an evolution toward lower energies. In Figures 2g–2j the fluxes in the keV range fell off while those near 100 eV (presumably originating from charge exchange within the coma and fairly near the spacecraft) increased and became more omnidirectional. By the time of Figures 2m and 2n, 9.5–10 UT, a broad beam centered at about 100 eV coming mostly from the solar direction (anodes 3–11) was established as the charge-exchange produced ions were picked up by the inflow. The emergence from the neutral density peak is somewhat different from the entry in Figures 2q–2v; the ~100 eV peak moved to higher energies while maintaining a beamlike nature. We conclude that as the neutral gas density at the SC location increased owing to the illumination conditions on the rotating nucleus, charge exchange was enhanced. The enhanced charge exchange caused degradation of the incoming beam and its replacement by more omnidirectional ions of lower energy, which then evolved into a low-energy beam as pickup commenced. As the neutral gas density at the spacecraft later decreased, the water-group ion beam was again observed near the keV range, as it was before the onset of the density enhancement. Notable in Figures 2c–2v are several instances of multiple energy-flux peaks, which could possibly have resulted from multiple ion species but owing to telemetry limitations, detailed mass spectra are not available to confirm their existence (see Figure S1 in Supporting Information S1). Contributing to the establishment of the ~100 eV beam in Figures 2m and 2n could have been an antisunward polarization electric field as predicted by Nilsson et al. (2018).

Further details of the ion distributions and their changes during the charge exchange and pickup process are shown in Figures 3 and 4. Figure 3 shows 3D maps of ion counts in CSEQ coordinates for time periods 07:30–

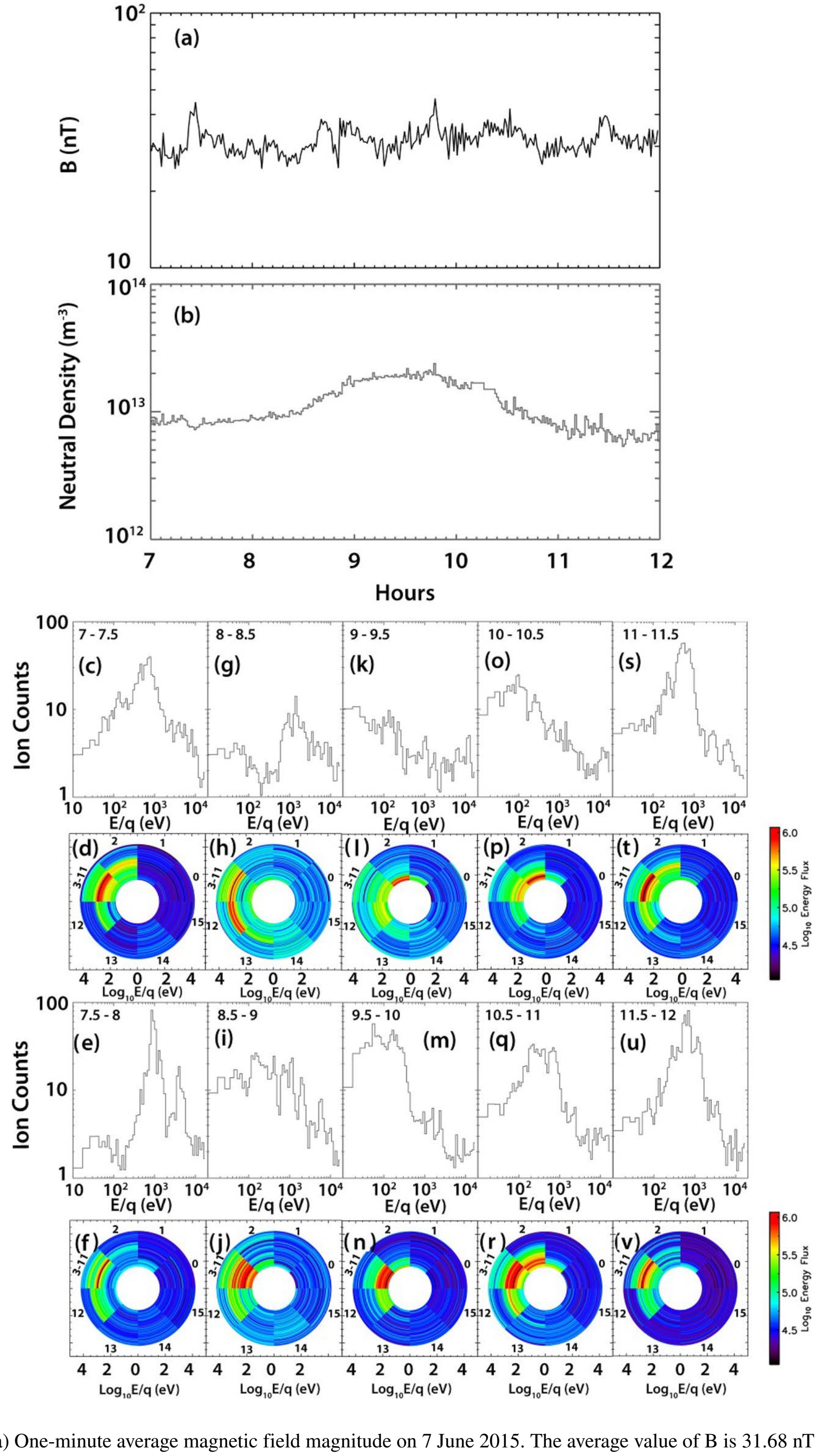

Figure 2. (a) One-minute average magnetic field magnitude on 7 June 2015. The average value of B is 31.68 nT with a standard deviation of 3.70 nT. (b) Neutral gas density (accuracy ∼20%). (c) Ion counts for 07–07.5 UT (proportional to energy flux) for Ion and Electron Sensor (IES) anodes 3–11 and IES elevation channels 04–08, which can be viewed near the solar direction. (d) Polar spectrogram showing ion energy flux for all anodes at elevation channels 04–08. (e) Same as (c) except for 07.5–08 UT. (f) Same as (d) except for 07.5–08 UT. (g–j) Same as (c–f) except for 08–09 UT. (k–n) Same as (c–f) except for 09–10 UT. (o–r) Same as (c–f) except for 10–11 UT. (s–v) same as (c–f) except for 11–12 UT.

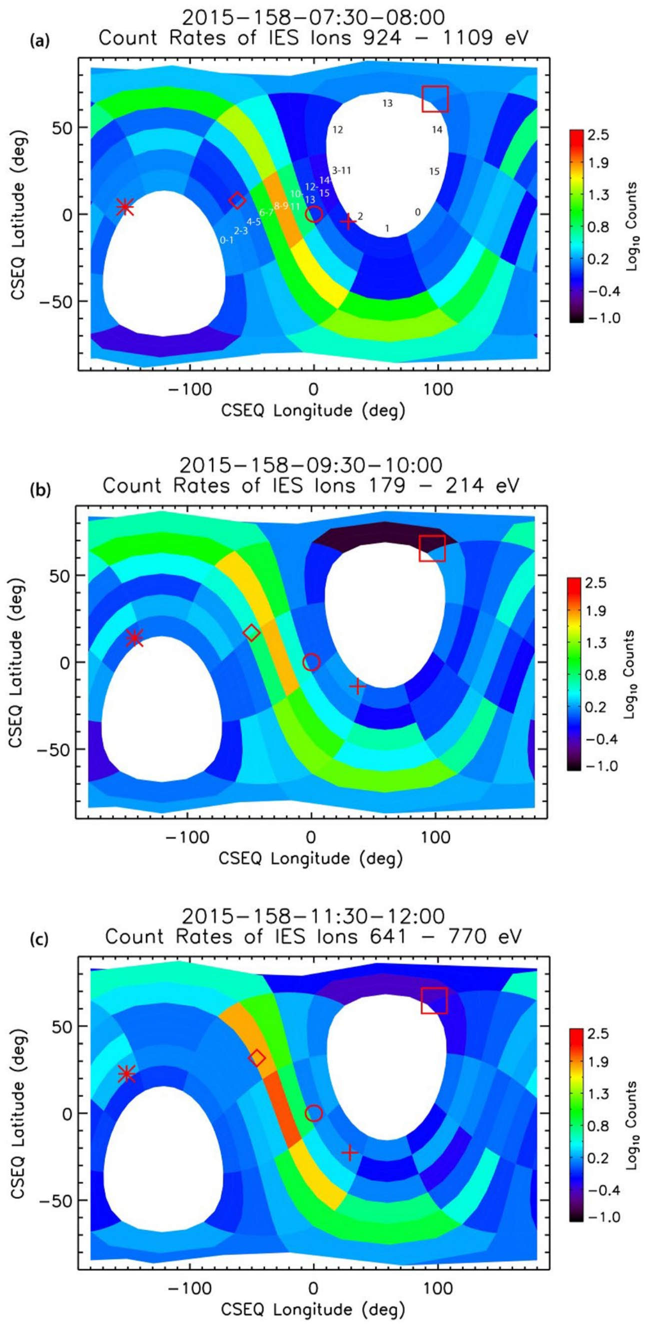

Figure 3. Count rates from all Ion and Electron Sensor (IES) ion channels at energy of peak count rate in Comet-Sun-Equatorial (CSEQ) coordinates on 7 June 2015 (day 158). Total field of view is 2.8**π** sr. Comet C-G direction is shown by the red square; Sun direction is shown by the red circle; magnetic field plus and minus directions are shown by the red plus sign and red asterisk, respectively; and (*b*x*v*)x*b* (a proxy for *E* x *B*) is shown by the red diamond. (a) Counts averaged over time period 07:30–08:00 UT and energy range 924–1109 eV/q with the IES elevation channel numbers noted in white and the anode numbers noted in black. (b) Time period 09:30–10:00 UT and energy range 179–214 eV/q. (c) Time period 11:30–12:00 UT and energy range 641–770 eV/q. Full energy range data are shown in movie format in Supporting Information S1.

08:00 UT, 09:30–10:00 UT, and 11:30–12:00 UT and at energies near the peak count rates. Data in Figure 3a were taken during the low-density time period before the density increase caused by the cometary rotation. Data in Figure 3b were taken during the increased neutral gas density. Finally, the Figure 3c data were acquired after the neutral gas density returned to near its initial low value. As shown in the titles of Figure 3, the energy at peak count rates varied from near 1 keV to near 200 eV to near 700 eV as the neutral density rose and then fell as the comet rotated during a 4.5-hr period. Such slowing down and speeding up of the solar wind has been observed during flybys of comets such as Grigg-Skjellerup (Coates et al., 1993) and Borelly (Young et al., 2004). The differences in the present event are: (a) the solar wind is already fully mass loaded, so only water-group ions are present and (b) the rotation of the comet allows for multiple measurements of mass loading and ion pickup processes to be observed in sequence.

The plots in Figure 3 show the fields of view and count rates of the various IES anodes (polar angles) and elevation channels, which are noted in Figure 3a. Also shown in Figure 3 are the directions to the Sun (open circle) and CG (square) along with the magnetic field vector (plus sign) and its negative (asterisk). Finally, the position in the IES field of view of pickup ions are drifting in the $E \times B$ direction as described by Coates (2004) (diamond). Since E is not measured on Rosetta, (bxv)xb is used as a proxy for $E \times B$ where b and v are unit vectors along B and the mass-loaded solar wind velocity, respectively. For simplicity, we have assumed a solar wind velocity along $-x_{cseq}$ (antisunward). In Figure 3, and especially for plots (b) and (c), the ions arriving from the $E \times B$ direction (the diamond symbol) are contained in or near the fields of view containing high ion fluxes. We conclude that ion pickup is active during the times of high neutral densities and later when the densities were lower. The difference being that for Figure 3b; the ke*V*-range ions have all been lost to charge exchange and replaced by picked-up cometary thermal ions. More evidence for this pickup explanation is shown in Figure 4, which shows ion energy flux versus Vpar and Vperp for the same three time periods as plotted in Figure 3. In Figure 4, the energy fluxes are those measured in elevation channels 8–9 because these channels contained the highest fluxes.

In each case in Figure 4, the edge of the yellow contours is near the Vperp axis, where initial pickup should occur (along $-v \times b$) and the fluxes extend toward the Vpar axis, becoming more intense with evidence of partial shell-like distributions, particularly in (c). The multiple velocity peaks seen in Figure 4 (a) and (c) could indicate a continuous pickup process as the ion distributions develop toward a single velocity. Alternatively, they could indicate different heavy-ion species since the velocities were derived under the assumption of 17 amu.

3. Charge Exchange Analysis

As determined by ICA, during the low-density portions of this event, the pickedup water-group ions at energies of about 1 keV/q were the only component of the solar wind to reach the spacecraft while the protons and alpha particles had been deflected around the solar wind cavity. During periodic passage through the higher density regions, charge exchange caused the ion energy to decrease owing to charge exchange between energetic ions and thermal neutral molecules followed by ion pickup. The ion E/q at peak flux

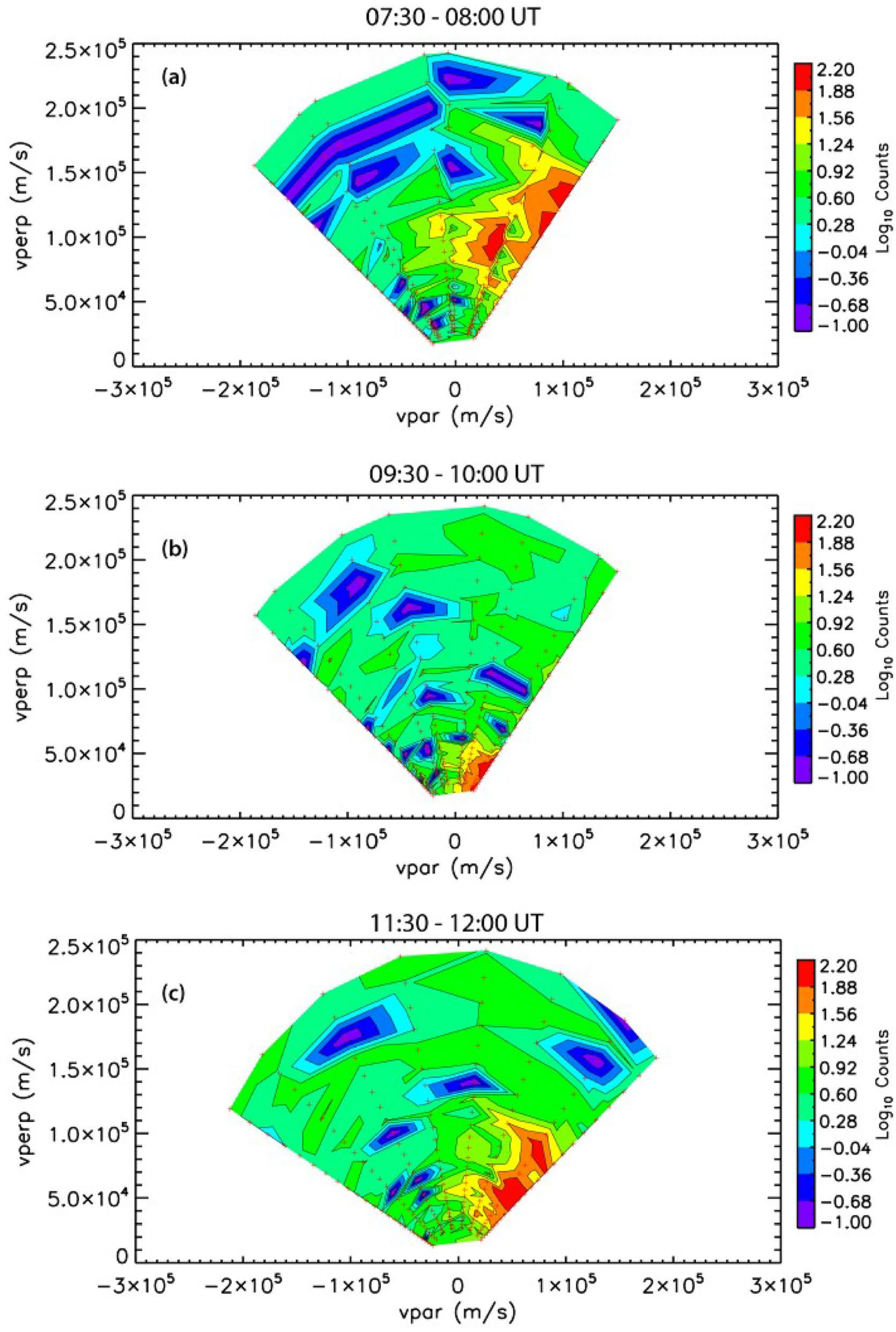

Figure 4. Ion counts versus Vpar and Vperp for Ion and Electron Sensor elevation channels 8–9 for the same three time periods as shown in Figure 4. (a) During low neutral gas density, (b) during maximum neutral gas density, and (c) during low neutral gas density.

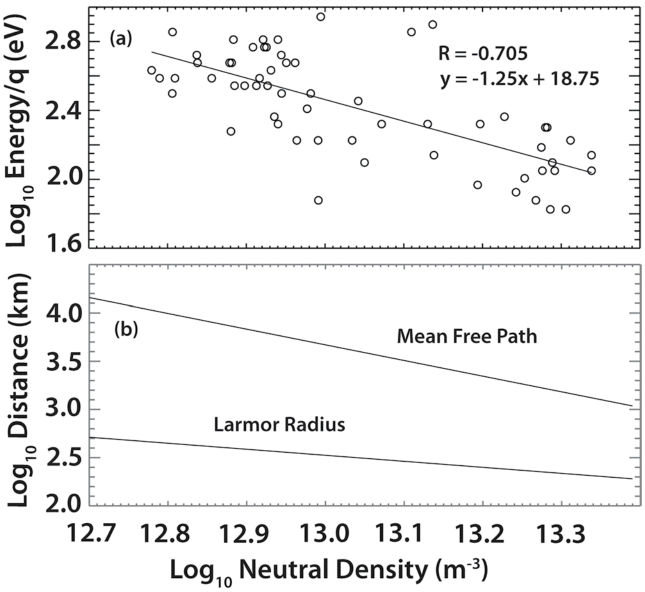

Figure 5. (a) Ion E/q at peak flux versus neutral density for 7–12 UT on 7 June 2015. (b) Mean free path and Larmor radius versus density using fit to (a) and mean magnetic field of 31.68 nT.

is plotted versus neutral density (n_n) for the time period 7–12 UT in Figure 5a along with a linear fit to the logarithmic data. The fit is a power law with

$$\mathrm{Log}_{10} E/q(eV) = -1.25\mathrm{Log}_{10} n_n \left(m^{-3}\right) + 18.75. \quad (1)$$

The simplest assumption for charge exchange is resonance (or symmetric) exchange involving water molecules:

$$H_2O + H_2O^+ \rightarrow H_2O^+ + H_2O^*, \quad (2)$$

where H_2O^* indicates energetic neutral molecules. Other charge-exchange reactions should also occur, including:

$$H_2O + H_2O^+ \rightarrow H_3O^+ + OH^*, \quad (3)$$

but for simplicity we confine our attention to reaction (Equation 2). Fleshman et al. (2012) and Lishawa et al. (1990) have reported an energy-dependent cross section (σ_{ce}) given by

$$\sigma_{ce} = 38.0 \left(E^{-0.5}\right) \text{ x } 10^{-16}\mathrm{cm}^2, \quad (4)$$

where E is the relative energy in eV between the energetic positive ion and the thermal neutral molecule. Using this cross section with E given by the power-law fit to Figure 5a, we computed the mean free path against charge exchange as a function of neutral gas density ($\lambda = 1/n\sigma_{ce}$) and plot it in Figure 5b. Also shown for comparison in Figure 5b is the Larmor radius of the ions using the energy from the fit to the data in Figure 5a and the average magnetic field magnitude from Figure 2a. We note in Figure 5b that at the highest densities at $R = 200$ km, the mean free path is still larger than the Larmor radius. For comparison, the charge-exchange lifetime ($\tau = 1/n\sigma_{ce}v$) over the density range of Figure 5 varies from 156 to 32s.

The subsequent analysis involves only the measurements within the density enhancement associated with the neck of the comet, that is, at the peak of the neutral density curve in Figure 3b. We assume the Haser (1957) model:

$$n_n = \frac{Q}{4\pi v_n R^2} \exp\left(\frac{-R}{t_{\mathrm{ion}} v_n}\right) \quad (5)$$

where n_n is neutral density, Q is the gas production rate, v_n is the neutral molecule velocity (assumed to be 0.7 km/s according to Gulkis et al., 2015), R is the distance from the comet, and t_{ion} is the ionization time of cometary neutrals ($\sim 8 \times 10^6$ s according to Vigren et al. (2015)). Since, as shown below, our analysis is limited to $R < 500$ km, the exponential term in Equation 5 can be neglected, yielding a simplified Haser model. Using the peak density in Figure 2b of $\sim 2 \times 10^{13}$ m^{-3}, we get Q of about 7×10^{27} s^{-1}, which agrees with previous estimates (e.g., Wedlund et al., 2019).

4. Conclusions

On 6–8 June 2015, the Rosetta Orbiter was near the dusk-side terminator of comet 67P Churyumov-Gerasimenko (CG) at a radial distance of ∼200 km from the comet and ∼1.48 AU from the Sun and was within the solar wind cavity as it was from 28 April to 15 December 2015. During the 6–8 June time period, there was evidence of a CME impact, which compressed the solar wind cavity so that the pickedup water group ions could then reach the SC. No protons or He^{++} were detected because they were deflected more strongly around the comet because of their lower momentum (Broiles et al., 2015).

Variations of neutral gas density were caused by the comet's rotation and the resulting changes of solar illumination of the nucleus. The spin axis of CG is such that gas (mostly water vapor) emanating from the neck region of the comet results in a neutral-density periodicity of one half the rotation period of 12.4 hr (Gulkis et al., 2015). While the density increase was only about a factor of two, it was enough to cause the keV-range water-group ion beam to degrade to a beam near 100 eV because of charge exchange within the coma. The newly created ions evolved into a low-energy (∼100 eV) antisolar beam as charge exchange was followed by pickup. These pickup ions were accompanied by ions resulting from the photoionization of coma neutral particles (Nicolau et al., 2017), which undergo the same pickup process but do not remove energetic ions from the flow. The transition out of the density enhancement was simpler since a new stream of ions in the keV range did not encounter the higher neutral densities.

Analysis of the evolution of ion energy with increased neutral gas density within the density enhancement allowed us to make estimates of the comet's gas production rate and the mean free path for charge exchange. We found that, while the mean free path decreased with increasing gas density, it still remained larger than the Larmor radius, which would allow the ion pickup process to work even at the highest densities.

Data Availability Statement

The data used for this report are available from the ESA data archive: https://archives.esac.esa.int/psa/#!Table%20View/Rosetta=mission and from the Small Bodies section of the NASA Planetary Data System: https://pds-smallbodies.astro.umd.edu/data_sb/missions/rosetta/index.shtml. The AMDA science analysis system (http://amda.cdpp.eu) is provided by the Centre de Donnés de la Physique des Plasmas, supported by CNRS, CNES, Observatoire de Paris, and Université Paul Sabatier, Toulouse, France.

Acknowledgments
Rosetta is a European Space Agency (ESA) mission with contributions from member states and the U.S. National Space Administration (NASA). The work on IES was supported by NASA through contract number 1345493 with the Jet Propulsion Laboratory, California Institute of Technology. The work on Rosetta Orbiter Spectrometer for Ion and Neutral Analysis was supported by the State of Bern, the Swiss National Science Foundation, and the ESA PRODEX Program. Work on ICA and Langmuir Probe was supported by the Swedish National Space Board. We thank the teams at Imperial College London and ESA who have been responsible for the operation of our instruments.

References

Balsiger, H., Altwegg, K., Bochsler, R. T. P., Rubin, M., Scherer, S., Wurz, P., et al. (2007). Rosina: Rosetta orbiter spectrometer for ion and neutral analysis. *Space Science Reviews*, *28*(2), 745–801. https://doi.org/10.1007/s11214-006-8335-3

Behar, E., Nilsson, H., Alho, M., Goetz, C., & Tsurutani, B. (2017). The birth and growth of a solar wind cavity around a comet - Rosetta observations. *Monthly Notices of the Royal Astronomical Society*, *469*(7), S396–S403. https://doi.org/10.1093/mnras/stx1871

Broiles, T. W., Burch, J. L., Clark, G., Koenders, C., Behar, E., Goldstein, R., et al. (2015). Rosetta observations of solar wind interaction with the comet Churyumov-Gerasimenko. *Astronomy and Astrophysics*, *383*(11), A21. https://doi.org/10.1051/0004-6361/201526046

Brueckner, G. E., Howard, R. A., Koomen, M. J., Korendyke, C. M., Michels, D. J., Moses, J. D., et al. (1995). The large angle spectroscopic coronagraph (LASCO). *Solar Physics*, *162*(1–2), 357–402. https://doi.org/10.1007/BF00733434

Burch, J. L., Goldstein, R., Cravens, T. E., Gibson, W. C., Lundin, R. N., Pollock, C. J., et al. (2007). RPC-IES: The ion and electron sensor of the Rosetta plasma consortium. *Space Science Reviews*, *128*(2), 697–712. https://doi.org/10.1007/s11214-006-9002-4

Coates, A. J. (2004). Ion pickup at comets. *Advances in Space Research*, *33*(11), 1977–1988. https://doi.org/10.1016/j.asr.2003.06.029

Coates, A. J., Johnstone, A. D., Huddleston, D. E., Wilken, B., Jockers, K., Borg, H., et al. (1993). Pickup water group ions at comet Grigg-Skjellerup. *Geophysical Research Letters*, *20*(6), 483–486. https://doi.org/10.1029/93GL00174

Edberg, N. J. T., Alho, M., André, M., Andrews, D. J., Behar, E., Burch, J. L., et al. (2016). CME Impact on comet 67P/Churyumov-Gerasimenko. *Monthly Notices of the Royal Astronomical Society*, *462*, S45–S56. https://doi.org/10.1093/mnras/stw2112

Edberg, N. J. T., Eriksson, A. I., Odelstad, E., Henri, P., Lebreton, J., Gasc, S., et al. (2015). Spatial distribution of low-energy plasma around comet 67P/CG from Rosetta measurements. *Geophysical Research Letters*, *42*(11), 4263–4269. https://doi.org/10.1002/2015GL064233

Eriksson, A. I., Boström, R., Gill, R., Ahlén, L., Jansson, S.-E., Wahlund, J. E., et al. (2007). RPC-LAP: The Rosetta Langmuir Probe instrument. *Space Science Reviews*, *128*(2), 729–744. https://doi.org/10.1007/s11214-006-9003-3

Fleshman, B. L., Delamere, P. A., Bagenal, F., & Cassidy, T. (2012). The roles of charge exchange and dissociation in spreading Saturn's neutral clouds. *Journal of Geophysical Research*, *117*(E5), E05007. https://doi.org/10.1029/2011JE003996

Galand, M., Héritier, K. L., Odelstad, E., Henri, P., Broiles, T. W., Allen, A. J., et al. (2016). Ionospheric plasma of comet 67P probed by Rosetta at 3 AU from the sun. *Monthly Notices of the Royal Astronomical Society*, *462*(11), S331–S351. https://doi.org/10.1093/mnras/stw2891

Glassmeier, K.-H., Richter, I., Diedrich, A., Musmann, G., Auster, U., Motschmann, U., et al. (2007). RPC-MAG the fluxgate magnetometer in the ROSETTA plasma consortium. *Space Science Reviews*, *128*(1–4), 649–670. https://doi.org/10.1007/s11214-006-9114-x

Goldstein, R., Burch, J. L., Mokashi, P., Broiles, T., Mandt, K., Hanley, J., et al. (2015). The Rosetta Ion and Electron Sensor (IES) measurement of the development of pickup ions from comet 67P/Churyumov-Gerasimenko. *Geophysical Research Letters*, *42*(5), 3093–3099. https://doi.org/10.1002/2015GL063939

Gulkis, S., Allen, M., von Allmen, P., Beaudin, G., Biver, N., Bockelée-Morvan, D., et al. (2015). Subsurface properties and early activity of comet 67P/Churyumov-Gerasimenko. *Science*, *347*(1), aaa709. https://doi.org/10.1126/science.aaa0709

Haser, L. (1957). Distribution d'intensité dans la tête d'une comète. *Bulletin de la Classe des Sciences de l'Académie Royale de Belgique*, *43*, 740–750.

Lishawa, C., Dressler, R. A., Gardner, J. A., Salter, R. H., & Murad, E. (1990). Cross sections and product kinetic analysis of H_2O^+-H_2O collisions at suprathermal energies. *The Journal of Chemical Physics*, *93*(5), 3196–3206. https://doi.org/10.1063/1.458852

Mandt, K. E., Eriksson, A., Beth, A., Galand, M., & Vigren, E. (2019). Influence of collisions on ion dynamics in the inner comae of four comets. *Astronomy and Astrophysics*, *630*(10), A48. https://doi.org/10.1051/0004-6361/201834828

Nicolau, G., Behar, E., Nilsson, H., Wieser, M., Yamauchi, M., Bercic, L., & Stenberg-Wieser, G. (2017). Energy angle dispersion of accelerated heavy ions at 67p/Churyumov-Gerasimenko: Implication in the mass-loading mechanism. *Monthly Notices of the Royal Astronomical Society*, *469*, S339–S345. https://doi.org/10.1093/mnras/stx1621

Nilsson, H., Gunell, H., Karlsson, T., Brenning, N., Henri, P., Goetz, C., et al. (2018). Size of a plasma cloud matters: The polarisation electric field of a small-scale comet ionosphere. *Astronomy and Astrophysics*, *616*, A50. https://doi.org/10.1051/0004-6361/201833199

Nilsson, H., Stenberg Wieser, G., Behar, E., Wedlund, C.-S., Gunell, H., Yamauchi, M., et al. (2015). Birth of a comet magnetosphere: A spring of water ions. *Science*, *347*(1), aaa0571. https://doi.org/10.1126/science.aaa0571

Vigren, E., Galand, M., Eriksson, A. I., Edberg, N. J. T., Odelstad, E., & Schwartz, S. J. (2015). On the electron-to-neutral number density ratio in the coma of comet 67p/churyumov–Gerasimenko: Guiding expression and sources for deviations. *The Astrophysical Journal*, *812*(1), 54. https://doi.org/10.1088/0004-637X/812/1/54

Wedlund, C. S., Behar, E., Nilsson, H., Alho, M., Kallio, E., Gunell, H., et al. (2019). Solar wind charge exchange in cometary atmospheres. iii. Results from the Rosetta mission to comet 67P/Churyumov-Gerasimenko. *Astronomy and Astrophysics*, *630*(10), A37. https://doi.org/10.1051/0004-6361/201834881

Young, D. T., Crary, F. J., Nordholt, J. E., Bagenal, F., Boice, D., Burch, J. L., et al. (2004). Solar wind interactions with Comet 19P/Borrelly. *Icarus*, *167*(1), 80–88. https://doi.org/10.1016/j.icarus.2003.09.011